



Research article

Nitrogen-doped ordered mesoporous carbon supported ruthenium metallic nanoparticles: Opportunity for efficient hydrogenolysis of biomass-derived 5-hydroxymethylfurfural to 2,5-dimethylfuran by catalytic transfer hydrogenation

Jibril Goli Buta^{*}, Bayisa Dame, Tariku Ayala*School of Mechanical, Chemical and Materials Engineering, Department of Chemical Engineering, Adama Science and Technology University, Adama, Ethiopia*

ARTICLE INFO

Keywords:

5-Hydroxymethylfurfural
2,5-Dimethylfuran
Biofuel
Catalytic transfer hydrogenation
Heterogenous catalysis
Nitrogen-doped mesoporous carbon
2%Ru-N-CMK-1

ABSTRACT

One of the most promising solutions to the current energy crisis is an efficient catalytic transformation of abundant low-cost renewable raw biomass into high-quality biofuel. Herein, a highly effective catalyst was constructed systematically for the selective synthesis of 2,5-dimethylfuran (DMF) biofuel from biomass-derived 5-hydroxymethylfurfural (HMF) via green catalytic transfer hydrogenolysis (CTH) using a nitrogen-doped ordered mesoporous carbon (N-CMK-1) decorated ruthenium (Ru)-based catalyst in *i*-propanol as hydrogen source. The structures and properties of different catalysts were characterized by different characterization techniques such as FTIR, XRD, N₂-sorption, CO₂-sorption, TGA, TEM, ICP-AES, CHNO analysis, and acid-base back titration. A complete HMF conversion with a high DMF yield of 88% was achieved under optimized reaction conditions. Regarding substrate conversion and product yield, the influence of reaction temperature, time, and hydrogen donors was thoroughly investigated. The nitrogen-promoted carbon support enhanced the dispersion of Ru due to the formation of appropriate basic site density which could efficiently promote the activation of alcohol hydroxyl in *i*-propanol and subsequent release of active hydrogen species. In the meantime, highly dispersed surface Ru nanoparticles (NPs) were beneficial for hydrogen transfer and activation of both carbonyl and hydroxyl groups in HMF. Moreover, Arrhenius kinetic analysis was studied by identifying 5-methyl furfural (5-MF) and 2,5-bishydroxymethylfuran (BHMF) as two key intermediates that dominate a distinct reaction pathway during hydrogenolysis of HMF to DMF via CTH. Furthermore, high stability without obvious loss of activity after three consecutive cycles was observed in a fabricated N-CMK-1 decorated Ru-based catalyst as a result of superior metal-support interaction and the mesoporous framework nature of the catalyst. These findings would not only offer a robust catalyst synthetic approach but also open a new avenue for the exploitation of biomass to specialty chemicals and advanced biofuels.

^{*} Corresponding author.

E-mail address: jibrilgoli430@gmail.com (J.G. Buta).

<https://doi.org/10.1016/j.heliyon.2024.e26690>

Received 27 October 2023; Received in revised form 14 February 2024; Accepted 18 February 2024

Available online 23 February 2024

2405-8440/© 2024 The Authors. Published by Elsevier Ltd. This is an open access article under the CC BY-NC-ND license (<http://creativecommons.org/licenses/by-nc-nd/4.0/>).

1. Introduction

Due to environmental and economic concerns associated with the depletion of petroleum reserves, a valorization of lignocellulosic biomass as a strategy to replace fossil resources is gaining growing interest this time. Catalytic approaches have emerged as a potential strategy for the transformation of plenty of these biomass resources into platform chemicals and advanced biofuels [1]. The platform molecule, 5-hydroxymethylfurfural (HMF) which can be obtained from the acid-catalyzed reaction of cellulosic biomass is one of the key precursors for the production of valuable chemicals and biofuels [2]. Notably, the presence of reactive structures such as C=O, C=C, C–O, and furan ring in HMF make it easily convert into different chemical derivatives. To mention a few, 2,5-dimethylfuran (DMF), 2,5-bishydroxymethylfuran (BHMF), 2,5-dimethyltetrahydrofuran (DMTHF), and 2-hydroxymethyl-5-methylfuran (MFA) are a chemical derivative which can be obtained from HMF by catalytic hydrogenation/hydrogenolysis reaction.

Among them, DMF holds great potential to produce a liquid fuel alternative when HMF is selectively hydrogenolyses catalytically. The desirable chemical and physical properties such as greater energy density, very low water solubility, high boiling range, and high research octane number make DMF the next-generation biofuel candidate [3]. Moreover, concerning their ignition, emission, and combustion properties, DMF has been effectively investigated as biomass-derived biofuels in a research engine, and their use was found to be quite acceptable in comparison to gasoline [4]. These extraordinary features make DMF a promising renewable biofuel for transportation. However, what remains a huge challenge for a highly efficient conversion of HMF into DMF is selective C–O bond cleavage.

Currently, to address the challenge, hydrogenolysis of HMF into DMF over non-noble metal-based catalysts particularly Cu, Ni, Co, and Fe has been reported under harsh reaction conditions [5–8]. However, they show poor selectivity and recyclability due to their deactivation problems [5,9–18]. In another case, various supported noble metal-based catalysts such as Pt, Pd, and Ru show high activity and selectivity for selective reduction of HMF into DMF under mild conditions [8,17–27]. Among the supported noble metal-based catalysts, Ru and Pd provided the best-reported performances [28]. However, as Pd-based catalysts are highly active for the hydrogenation of C=O, C=C bonds of furan ring, and hydrogenolysis of C–O bonds, result in a moderate DMF selectivity [29]. Moreover, the scale-up application is also limited due to the high costs of Pd. On the contrary, as a less expensive noble metal, supported Ru is the most efficient catalyst in the liquid-phase hydrogenation of bio-sourced molecules to achieve a rapid and selective conversion of furanyl platform compound [30,31]. Even though Ru-based catalysts could improve the selectivity of DMF, their stability is not, however, satisfactory due to considerable migration and deactivation even after the first run [32]. Thus, it is desirable to develop a stable Ru catalyst for selective hydrogenation of furanyl compounds, which still is a challenging task.

Moreover, a high-pressure external molecular gas, (H_2) [33–38] is used as a reducing agent with the promotion of either Lewis acid or Brønsted acid as co-catalysts to catalyze HMF to DMF over noble/non-noble metals catalysts [39–41]. However, the use of high-pressure H_2 would certainly cause several drawbacks such as large-scale storage risk, transportation, and safety risks. Also, the solubility of H_2 in the reaction medium may limit the rate of liquid phase hydrogenation of HMF and need costly high-pressure operation. Furthermore, the potential utilization of acid promoters could undoubtedly require corrosion resistance equipment, thus, its use will add cost to the process and make the process less green and environmentally unfriendly. Additionally, it is also difficult to separate a homogeneous acid co-catalyst from the reaction mixture and a harsh reaction condition may lead to undesired furan-ring saturation. In practice, for the production of drop-in fuels and specialty chemicals from lignocellulosic biomass, it is desirable to avoid acid co-catalysts and minimize high-pressure external H_2 gas, especially if H_2 is being obtained from fossil fuels. Thus, the development of a highly efficient and stable Ru metal catalyst that could catalyze HMF to DMF without relying on external H_2 is highly demanding.

Recently, an interesting alternative to the hydrogenation of biomass-derived molecules using molecular H_2 known as the catalytic transfer hydrogenation (CTH) route using liquid molecules such as *i*-propanol, ethanol, formic acid, butanol, and cyclohexanol has been reported [3]. In this regard, among different types of hydrogen donors, alcohols served as potential H-donors. Polar alcohols including *i*-propanol, ethanol, and methanol are commonly used as the reaction media for hydrogenation of furanyl compounds with *i*-propanol being the most often selected alcohol for such chemistries [42,43]. Moreover, these low-carbon alcohols can determine the catalytic transfer hydrogenation pathway via their hydrogen-donating ability, act as surface ligands of metals via strong dissociative adsorption, and change their steric hindrance to regulate the transient states of the reaction intermediates [44].

A typical method to improve the stability of supported metal catalysts is by changing the surface chemistry of supports. Recently, carbon materials modified with nitrogen(N)-doping have exhibited superior catalytic performance for applications such as heterogeneous catalysis as catalyst support [45], aqueous phase reforming [46], supercapacitors [47], metal-free oxygen reduction reaction [48], oxidation reaction [49], hydrogenation and hydrogenolysis reactions [50]. Compared to undoped counterparts, N-doping alters the chemical and physical characteristics of carbon materials by enhancing the support–metal nanoparticles binding interaction and increasing the number of catalytic active sites [51,52]. This can be witnessed in terms of an increased metal dispersion, higher resistance to metal sintering and enhanced catalytic performance [53,54]. Interestingly, carbon materials functionalized with different N groups can enhance the dehydrogenation ability of hydrogen donor compounds by adsorbing a proton from alcohol via basic sites brought by nitrogen dopants [55,56].

Based on the aforementioned information, in this work, an efficient alternative process for the selective hydrogenolysis of HMF to DMF via CTH reaction was reported by employing *i*-propanol as a solvent and hydrogen source, where in the process, a nitrogen-doped mesoporous carbon-supported Ru metallic nanoparticles were used as a catalyst without the need for a Brønsted acid co-catalyst.

2. Experimental section

2.1. Materials and chemicals

Nitric acid (70–71%, Aencore Chemical Co., LTD.), Urea for electrophoresis (99%, Sigma-Aldrich), *i*-propanol (HPLC grade, J.T. Baker), 5-hydroxymethylfurfural; 5-HMF (98%, AK scientific), 2,5-Bis (hydroxymethyl)furan; BHMF (98%, AK scientific); 2,5-dimethylfuran; 2,5-DMF (99%, Acros); 2,5-Dimethyltetrahydrofuran; DMTHF (mixture of *cis*- and *trans*-, 96%, Sigma-Aldrich); 5-Methylfurfural (5-MF, 99%, Sigma-Aldrich), 5-Methyl-2-furanmethanol; MFA (97%, Acros), Ruthenium chloride n-Hydrate (39% metal content, UniRegion Bio-Tech), Hydrogen fluoride (HF, 48% Sigma-Aldrich), Hydrochloric acid ($\geq 37\%$, Honeywell Fluka), Ethanol (99.9%, Honeywell Riedel-de-Haën), Aluminum (III) Chloride (98%, Sigma-Aldrich), Poly (ethylene glycol)-*b*-poly (propylene glycol)-*b*-poly (ethylene glycol), Pluronic P123 (Sigma-Aldrich), Furfuryl alcohol; FUL (98%, Acros Organics), Tetraethyl silicate (98%, Sigma-Aldrich), Ammonium hydroxide (28–30%, JT Baker Chemicals), Cetyltrimethylammonium bromide (98%, Alfa Aesar), Pluronic F-127 (Sigma-Aldrich). Unless otherwise stated, all chemicals were used as received without further purification.

2.2. Preparation of catalyst

- (a) **Synthesis of MCM-48:** MCM-48 silica nanoparticle was prepared according to previously reported literature [57]. Briefly, 3.7 g of CTAB (Cetyl Trimethyl Ammonium Bromide), 15.0432 g of F-127, and 709.7946 g of deionized (DI) water, 74.5256 g of NH_4OH (29%) and 252.5665 g of Ethanol were added into 2 L plastic mixing tank one after the another and stirred at 450 rpm for 1 h. The well-dispersed solution was mechanically stirred from 0 to 1000 RPM and 13.2189 g of TEOS was added at once, where it was kept for 1min at 1000 RMP. Then, the resulting solution was kept in a low-temperature incubation under static conditions at 25 °C for 24 h for further silica condensation. The white solid product was recovered by ultrahigh-speed centrifuge (10,000 RPM, 30min, 4 °C) three times. For the post-hydrothermal synthesis, the centrifuged sample was placed in a Teflon-lined autoclave with 30 mL of DI water and mixed to disperse uniformly. The solution was kept in a conventional oven at 150 °C for 48 h under static conditions. After cooling down to room temperature, the product was centrifuged (10,000 RPM, 30 min, 4 °C) two times. The collected product was calcined in a muffle furnace at 550 °C for 2 h at a rate of 1.5 °C/min for the removal of surfactant.
- (b) **Synthesis of Al-MCM-48:** 10 mL of anhydrous ethanol was added to 1 g of MCM-48 and the solution was stirred at 400 rpm for 10 min. The Al precursor, AlCl_3 (0.111 g) was added to the above solution and the mixture was continuously stirred at room temperature for 1 h. Ethanol was completely removed by a rotary vacuum evaporator. The Al-containing MCM-48 was further dried in a muffle furnace at 100 °C for 5 h. The dried sample was calcined at 550 °C, 1.5 °C/min for 2 h to incorporate Al on the surface of silica.
- (c) **Synthesis of Ordered Mesoporous Carbon (CMK-1):** CMK-1 nanomaterial was prepared using furfuryl alcohol as carbon precursor and Al-MCM-48 silica as a hard template. Accordingly, 3.0166 g of silica was infiltrated with 3.00229 cm^3 furfuryl alcohol by vortexing and kneading at room temperature. The mixture was transferred into the Schlenk reactor and subjected to a freeze-vacuum-thaw process three times using liquid nitrogen. It was frozen for 5 min and vacuum-thawed for 10 min at each cycle. The mixture was kept under vacuum at 35 °C for 1 h in a conventional oven to uniformly distribute carbon precursor into the pores. To polymerize the furfuryl alcohol inside the silica pores, the Schlenk reactor was opened, and the mixture was heated in the same oven at 90 °C for 6 h. Then, the powder was transferred into a tube furnace for partial carbonization under vacuum at 350 °C for 3 h. After cooling to room temperature, 60% volume of furfuryl alcohol to the total pores volume of the template was added and repolymerized by repeating the freeze-vacuum-thaw process. The sample was fired in a tubular furnace under vacuum at 350 °C for 3 h and the furnace temperature was subsequently increased to 900 °C for 2 h for complete carbonization. The silica-carbon nanocomposite material was washed with 10 wt% HF in ethanol-water solution (twice) to remove the silica. Finally, the sample was filtered, washed with ethanol, and oven dried at 120 °C for 12 h.
- (d) **Synthesis of Nitrogen-doped ordered mesoporous carbon (N-CMK-1):** Before nitrogen-doping, the surface of CMK-1 was functionalized with surface oxygen groups [58]. Typically, CMK-1 (350 mg) was treated with 105 mL of HNO_3 (8 M) by vigorously stirring at 600 RMP for 3 h at 80 °C, under reflux conditions. After treatment, the obtained sample was recovered by filtration and washed thoroughly with DI water and ethanol until neutral. The solid product was oven-dried at 80 °C for 12 h. Subsequently, acid-treated CMK-1 (O-CMK-1) was modified with heteroatom nitrogen, where urea was used as both a reducing agent and chemical dopant. Here, O-CMK-1 (100 mg) was diluted with 25 mL of DI water and the solution was allowed for sonication for 30 min. Then, carbon to urea mass ratio (1:300) and DI water (62.5 mL) was added into the O-CMK-1 dispersion and the sonication continued for another 2.5 h. Subsequently, the solution was transferred and sealed in a Teflon-lined autoclave and maintained at 180 °C for 12 h. The N-doped CMK-1 was filtered and washed several times with water and ethanol until the pH became neutral. Finally, the collected sample was oven-dried at 80 °C for 12 h and labeled as N-CMK-1. For comparison, the oxygen-functionalized mesoporous carbon (O-CMK-1, HT, no Urea) was prepared under the same experimental conditions without adding the urea.
- (e) **Synthesis of carbon-supported ruthenium catalysts:** Ruthenium chloride with 2 wt% was mixed with 100 mg of porous carbon supports (CMK-1 and N-CMK-1) in 10 mL of *i*-propanol at 62 °C for 3 h and the mixture was stirred at 600 rpm under nitrogen environment. Subsequently, the solvent was removed by a rotary vacuum evaporator, and the solid mixture was freeze-dried for 36 h. The collected mixture was placed on a quartz boat in a tube furnace and treated with constant hydrogen flow (100 mL min^{-1}) to reduce the metal precursor into its metallic form. The reduction process was programmed as follows: from

room temperature to 300 °C at a rate of 2 °C/min and held at this temperature for another 3 h. Continuously, the as-synthesized material was cooled to room temperature under hydrogen flow and followed by nitrogen flow. The finally collected sample was labeled as 5%Ru-N-CMK-1, 2%Ru-N-CMK-1. For comparison, nitrogen-free porous carbon was also prepared in a similar fashion and labeled as 2%Ru-CMK-1 and 5%Ru-CMK-1.

2.3. Materials characterization method

Fourier-transform infrared spectroscopy (FT-IR) was obtained on a PerkinElmer spectrometer with attenuated total reflection mode. Before the spectral measurement, the sample was ground with KBr powder and then the spectra were recorded in the range of 4000–650 cm^{-1} with a fixed scan rate of 100 and 4 cm^{-1} resolution. Powder X-ray diffraction (PXRD) was obtained by Bruker D8 ADVANCE X-ray diffractometer to record powder XRD pattern using Cu $K\alpha$ source radiation ($\lambda = 1.5406 \text{ \AA}$) over the scanning angle (2θ) range from 0.5° to 5° (for small angle) and 10 to 70° (for wide angle) operated at 40 kV and 40 mA with a constant scanning rate of 0.5 s. Nitrogen sorption analysis was obtained by a Micromeritics 3-Flex volumetric adsorption analyzer. Before sorption analysis, all the samples were degassed at 90 °C for 1 h and then at 150 °C for 6 h, under vacuum conditions. Then, the isotherms are measured under liquid nitrogen (77 K). Specific surface area, total pore volume, and pore size distribution of the mesoporous materials are respectively obtained by the Brunauer–Emmett–Teller (BET) equation, amount of nitrogen adsorbed at $P/P_0 = 0.95$ and the Barret-Joyner-Halenda (BJH) method. Thermogravimetric analysis (TGA) was acquired by a thermogravimetric analyzer (Pyris 1, PerkinElmer) to carry out the thermal analysis. After degassing at 120 °C for 0.5 h, approximately 7 mg of the sample was heated from 30 °C to 900 °C, 10 °C/min under a nitrogen environment (35 mL min^{-1}). The elemental composition of the materials was determined by an elemental analyzer Instrument, an elementary Vario EL cube (for NCSH, German). For the estimation of C, N, H, and Oxygen, Acetanilide and Benzoic acid were respectively used as external standards. Inductively coupled plasma optical emission spectroscopy was used to determine the actual concentration of ruthenium in each support (ICP-AES, Agilent 725, USA). Through a microwave-assisted temperature-programmed treatment, the metal-containing liquid solution was obtained after digesting the solid catalysts with 4 mL nitrohydrochloric acid. Subsequently, the temperature was programmed to 170 °C at a ramping rate of 9.3 °C/min, followed by a 20-min brief dwell. A high-temperature treatment was then applied to the solution at 190 °C for another 20 min at a ramping rate of 4 °C/min from 170 °C to 190 °C. The metal-containing solutions were diluted 10.5 times with DI water after acid digestion prior to ICP-AES analysis. Acid–base back titration method was used to quantify the total surface acidity and basicity. Consequently, to determine the total surface basicity, 50 mg of material was vortexed in 20 mL of 0.01 N HCl aqueous solution for a period of 2 h. Subsequently, after collecting the solid by filtration and washing with 10 mL of water, the filtrate was titrated with 0.01 N aqueous NOH solution, using phenolphthalein as an indicator. Using a similar fashion but titrating the filtrate against 0.01 N HCl aqueous solution was employed to determine the total acidity.

2.4. Catalytic performance test

The catalytic transfer hydrogenolysis reaction of 5-HMF to 2,5-DMF was carried out using the Biotage Reactor (Biotage Endeavor Catalyst Screening System) under programmed experimental conditions. A 4 mL of 20 mM of 5-HMF in *i*-propanol with 10 mg of the catalyst was charged into a glass liner reactor. After the reaction, the eluent was filtered and submitted to a Gas Chromatograph (GC-2014, Shimadzu, Japan) equipped with a flame ionization detector (FID) and a 30 m capillary column (SH-RXI 5MS, Shimadzu) for the quantification of unreacted feed and desired products. The vaporization of the aliquot (1 μL) of resulting solutions has occurred at 200 °C up on injection and the separation was programmed as: (a) ramping up (40 °C/min) from the initial temperature of 40 °C–115 °C after 5 min of equilibration, followed by (b) ramping up (20 °C/min) from 115 °C to 150 °C after 2 min of equilibration. Carried by Helium gas with a steady flow of 1.3 mL min^{-1} , the sample would reach the FID detector for complete combustion at 250 °C. After

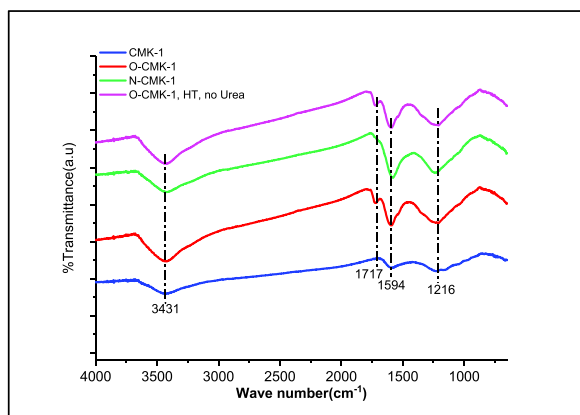


Fig. 1. FTIR spectra for Pristine carbon (CMK-1), Oxygen functionalized CMK-1(O-CMK-1), Nitrogen-doped CMK-1(N-CMK-1) and Oxy-functionalized-hydrothermally treated without urea, (O-CMK-1, HT, no Urea).

quantitatively quantifying the products by using GC-FID, the conversion of HMF and the product yield were calculated by Ref. [59]:

$$\text{HMF conversion (\%)} = 1 - \left(\frac{\text{mole of HMF in product}}{\text{starting mole of HMF}} \right) \times 100 \quad (1)$$

$$\text{Product yield (\%)} = \left(\frac{\text{mole of product}}{\text{starting mole of HMF}} \right) \times 100 \quad (2)$$

3. Results and discussion

Fourier transform infrared (FT-IR) spectroscopy was employed to identify the functional groups present in the materials. The generation of the abundant surface oxygen-containing group is always accompanied by the oxidation treatment of carbon materials [60]. As shown in Fig. 1, the generated surface oxide/nitridation respectively by HNO_3 wet oxidation and reduction by urea were detected by FT-IR surface spectra. All samples experience the broadband centered at about 3431 cm^{-1} which is mainly assigned to O-H stretching vibration of adsorbed water molecules.

After surface modification, increased intensity of the existing bands, the appearance of several new bands, and the disappearance of several bands were prominent. The increased intensity of the band at 3426 cm^{-1} was observed for O-CMK-1. This was because nitric acid oxidation produces more surfaces -OH group from newly emerged carboxyl and phenolic groups [60]. The new intense band at 1717 cm^{-1} for the O-CMK-1 sample is attributed to the generation of high-density carboxylic groups. Most importantly, the generation of a new band at 1216 cm^{-1} can be assigned to the C-O bonds from ester, phenolic, and etheric groups, suggesting the generation of numerous oxygen functional groups. For N-CMK-1, the FT-IR spectra show that the reduction of peak at band 1717 cm^{-1} and appearance of intense peak at 1216 cm^{-1} bands which assure that during hydrothermal treatment, oxy groups on O-CMK-1 has been successfully reduced by urea to obtain N-CMK-1 by replacing oxygen atoms with nitrogen atoms. So, the peaks that appeared at 1216 and 1602 cm^{-1} in N-doped CMK-1 could correspond to C-N and C=N stretching vibration, respectively [61]. For the sample hydrothermally treated without urea (O-CMK-1, HT, no Urea), the IR spectra did not show any change to that of oxygen functionalized carbon (O-CMK-1), confirming the double roles of urea as both reducing agent and nitrogen dopant.

The X-ray diffraction pattern (XRD) of the catalytic materials and their corresponding 2%Ru loading are shown in Fig. 2. For CMK-1 derived materials, the small angle XRD pattern depicts a typical diffraction at (100), (211), and (220) reflection [62] with slightly reduced peak intensity from pristine to N-doped carbons through their corresponding ruthenium loaded counterparts (Fig. 2a). Compared to pristine CMK-1, the reduction in peak intensity was seen in nitrogen doped, and its ruthenium loaded-counterpart. This may be attributed to the structural damage during acid treatment, the incorporation of heteroatom nitrogen in the carbon framework, and the creation of surface defects during nitrogen doping. It is noteworthy that, acidic surface oxidation, subsequent oxygen removal-nitrogen doping process by urea during hydrothermal treatment, and final ruthenium metallic nanoparticles loading did not cause a severe carbon wall structural disordering. Moreover, a wide-angle XRD (Fig. 2b) pattern of pristine mesoporous carbon, nitrogen-doped, and their corresponding 2%Ru catalysts were demonstrated and display similar XRD characteristics where a

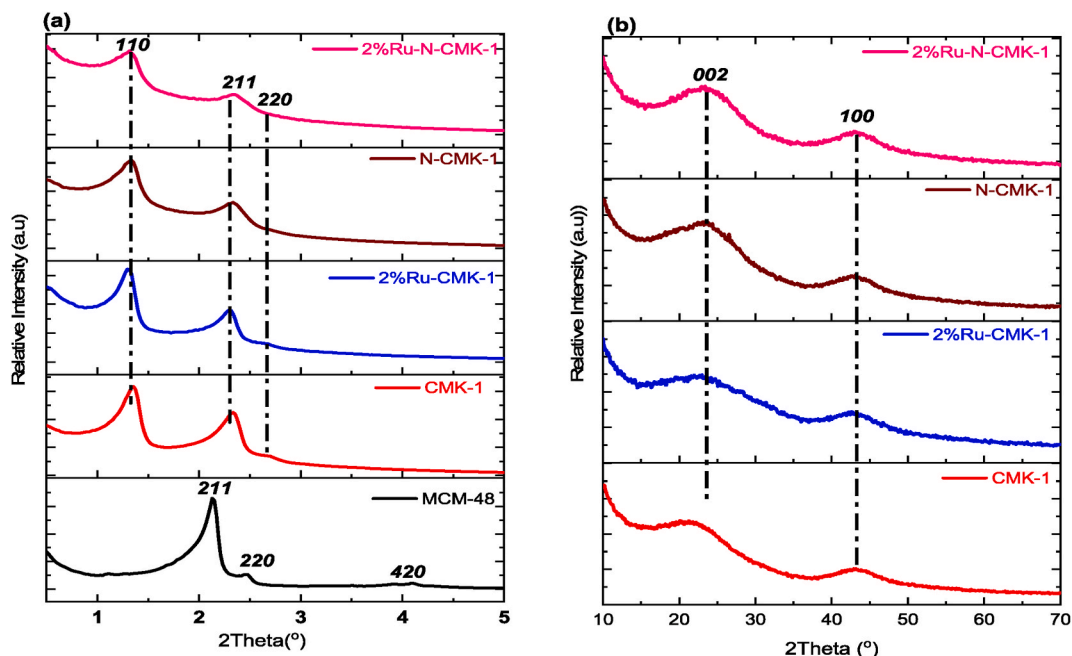


Fig. 2. Small (a) and Wide angle (b) XRD for Pristine CMK-1, N-CMK-1, and their corresponding 2%Ru loading.

noticeable peak at nearly $2\theta = 22.9^\circ$ and 43.02° , are respectively related to the (002) and (100) planes of graphitic carbon materials [63]. Interestingly, the Ru-loaded supports did not show any noticeable characteristic diffraction peaks that correspond to ruthenium nanoparticles (either metallic Ru⁰ or Ru oxides) indicating a high dispersion of Ru metal on the supports. Surprisingly, neither nitrogen doping nor Ru loading alters the diffraction and position of the two peaks.

The thermal properties of CMK-1, O-CMK-1, N-CMK-1, and ruthenium-supported nitrogen-doped carbon were investigated by TGA analysis and all materials showed nearly similar decomposition behavior (Fig. 3a). The initial weight loss in all cases is attributed to the presence of water molecules trapped in the catalysts pore. It shows for O-CMK-1, the major weight loss which is recorded from 180 to 310 °C, might be attributed to the decomposition of different oxygen functionalities such as carboxylic and phenolic groups [60]. The mass loss above this temperature might be assigned to either the decomposition of lactone and ether or further decomposition of oxygen-containing groups and self-combustion of the carbon network because of the existence of small amounts of oxygen. Compared to oxygen-functionalized porous carbons, the curves of nitrogen-doped carbon were quite stable throughout the tested temperature range, indicating the removal of oxygen functional groups during hydrothermal treatment. Moreover, according to TGA data, compared to others, the ruthenium-loaded nitrogen-doped carbon material has shown better thermal stability. Thus, it can be concluded that the synthesized catalyst is thermally stable and suitable for hydrodeoxygenation of HMF to DMF. Furthermore, a similar phenomenon of the decomposition behavior is obtained from the 1st derivative TGA curve (Fig. 3b). Reduction in thermal decomposition point from CMK-1 to O-CMK-1 through N-CMK-1 pinpoints the introduction of oxy and nitrogen functionality. It can be seen that for Ru-loaded N-CMK-1, a highly stable thermal decomposition behavior, which suggests that oxygen functionalities had been removed and the pendant amino groups were converted to highly stable forms of other nitrogen functionalities during thermal reduction of the catalyst with H₂.

MCM-48 and All CMK-1 derived materials show similar type IV(b) isotherm [64], signifying the mesoporous nature of silica and carbon materials after oxygen functionalization, subsequent nitrogen doping during hydrothermal treatment process and final Ru NPs loading (Fig. 4a). However, a small drop in surface area (Table 1) was apparently observed after nitrogen doping, which might be attributed to the minor collapsing of the pore wall during the subsequent removal of oxygen functionalities and nitrogen doping during hydrothermal treatment with urea. Also, upon ruthenium metal loading, there has been a noticeable small drop in BET surface area; which could correspond probably to partial blockage of micropores by entrapped Ru NPs. Their pore size distribution is very similar from 2.15 to 2.45 nm range of mesoporous materials (Fig. 4b and Table 1). The textural and physiochemical properties of the synthesized materials are summarized in Table 1.

The basicity of N-doped carbon materials was investigated by the acid-base back titration method (Table 1). All N-doped samples show a quantifiable amount of basic density. This result confirms the presence of basic site density due to nitrogen functionalities, with the basicity values of 2.0112, 1.5288, and 1.1345 mmol g⁻¹ respectively for N-CMK-1, 2%Ru/N-CMK-1 and 2%Ru/N-CMK-1 (Reused) catalysts. These results imply that increasing the nitrogen contents of the sample will result in the enhancement of the basicity of the carbon sample.

Furthermore, the morphological structure of the samples was confirmed by transmission electron microscopy (TEM) (Fig. 5). From the TEM image observation, a uniform pore distribution is revealed in CMK-1 with no carbon deposition on the external and internal surfaces (Fig. 5a). However, somehow dissimilarity was observed for N-CMK-1 (Fig. 5b), which may imply the effect of pore wall structural disordering and surface defect due to subsequent oxidation and amination reaction respectively by HNO₃ and hydrothermal urea treatment process. Furthermore, the size of ruthenium metallic nanoparticles and their distribution were investigated by TEM image (Fig. 5 d, f, h). It was found that with 2%Ru-CMK-1, Ru metallic NPs are unevenly distributed; however apparent agglomeration of Ru average particle size of approx. 2.75 nm was seen (Fig. 5d). With 2%Ru-N-CMK-1, it was clear that ruthenium metallic nanoparticles were dispersed homogeneously with an average particle size of 1.41 nm (Fig. 5f). It was also noted that from TEM image, for

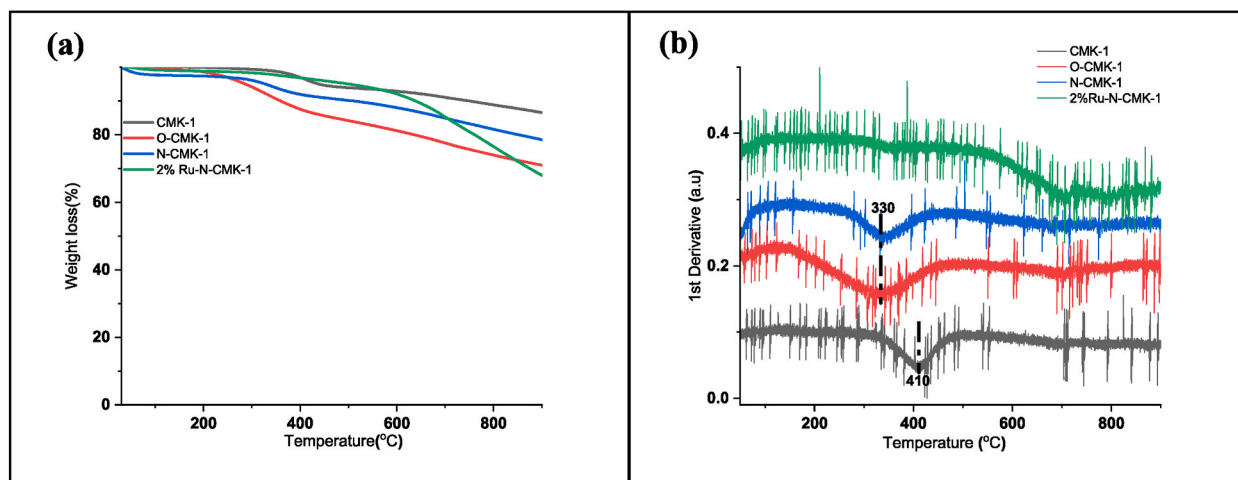


Fig. 3. Weight loss TGA Curve (a) and first derivative TGA curve (b) for CMK-1, O-CMK-1, N-CMK-1 and 2%Ru-N-CMK-1.

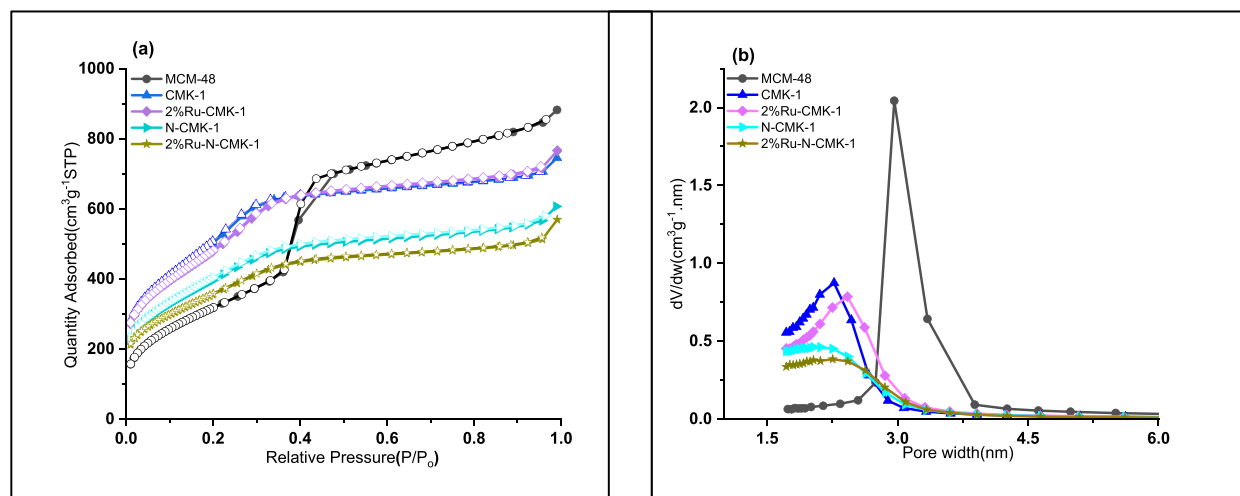


Fig. 4. N₂ sorption isotherm (a) and Pore size distribution (b) for CMK-1, 2%Ru-CMK-1, N-CMK-1, 2%Ru-N-CMK-1 and MCM-48.

Table 1

Textural and physio-chemical properties of the materials.

Catalysts	BET surface area ^a (m ² g ⁻¹)	Total pore volume ^a (cm ³ g ⁻¹)	Pore Width ^a (nm)	Ru content ^b (wt%)	Avg. Ru particle size ^c (nm)	Nitrogen content ^d (wt%)	Basicity ^e (mmol g ⁻¹)
CMK-1	1890	1.1124	2.33	–	–	–	–
2%Ru/CMK-1	1751	1.0470	2.42	1.980	2.75	–	–
N-CMK-1	1453	0.8820	2.15	–	–	6.05	2.0112
2%Ru/N-CMK-1	1288	0.7930	2.23	1.970	1.41	5.5	1.5288
2%Ru/N-CMK-1 (Reused)	1097	0.6820	2.33	1.968	1.52	5.1	1.1345

^a Determined from N₂-physisorption.

^b Estimated by ICP-AES.

^c Calculated from TEM analysis.

^d Calculated using elemental analysis.

^e Determined by acid-base back titration.

the sample used after third cycles, 2%Ru–N-CMK-1 (reused), with average ruthenium particle size of 1.52 nm, nearly the same as size of fresh catalyst. Therefore, it can be concluded that the nitrogen in the carbon framework structure plays a pivotal role in stabilizing Ru NPs where increasing the nitrogen level in the carbon framework results in smaller Ru NPs and vice versa [46].

By taking into consideration the shape of ruthenium as a spherical NPs and using the equation given by Scholten et al. [65], ruthenium dispersion (%) was determined based on the average Ru particle size on supported Ru catalyst: [65]

$$D = 10^{21} \frac{6 \times M \times \rho (\text{metal surface})}{d \times \rho (\text{metal}) \times N} \quad (3)$$

Where, Ru metal dispersion (%) = Ru metal dispersion (D) × 100.

D = Ru metal dispersion.

M = Ru atomic weight (101 g mol⁻¹).

$\rho(\text{metal surface site})$ = Ru metal surface site density (16.3 atoms (nm²)⁻¹).

d = average Ru metal particle size estimated from TEM (nm).

$\rho(\text{metal})$ = Ru metal density (12.3 g (cm³)⁻¹).

N = Avogadro constant, giving D = 1.33 d⁻¹ (nm) for Ru.

The calculated ruthenium dispersion values were 48.65 for 2%Ru-CMK-1 and 94.57% for 2%Ru-N-CMK-1. The improved ruthenium dispersion over nitrogen-modified support witnessed the uniform deposition of Ru metallic NPs. Previous studies indicated well dispersion of metallic NPs supported on carbon materials with N doping compared to the un-doped ones [66,67]. For example, Warczynski et al. have confirmed that the loading of Pd NPs on N-doped mesoporous carbon led to a better dispersion of Pd compared to those for Pd supported on N-free mesoporous carbon [68]. However, it can be seen that, after the third run (2%Ru/N-CMK-1, reused), the % dispersion slightly reduced to 87.56 value (Table 2), which corroborates the result of TEM analysis. Thus, it can be strongly agreed from TEM data and % dispersion calculation that, the enhancement of nitrogen content in the carbon catalyst, could result in the dispersion of Ru metallic NPs and suppress the aggregation [69]. It was demonstrated by Garcia-Bordejé et al., that

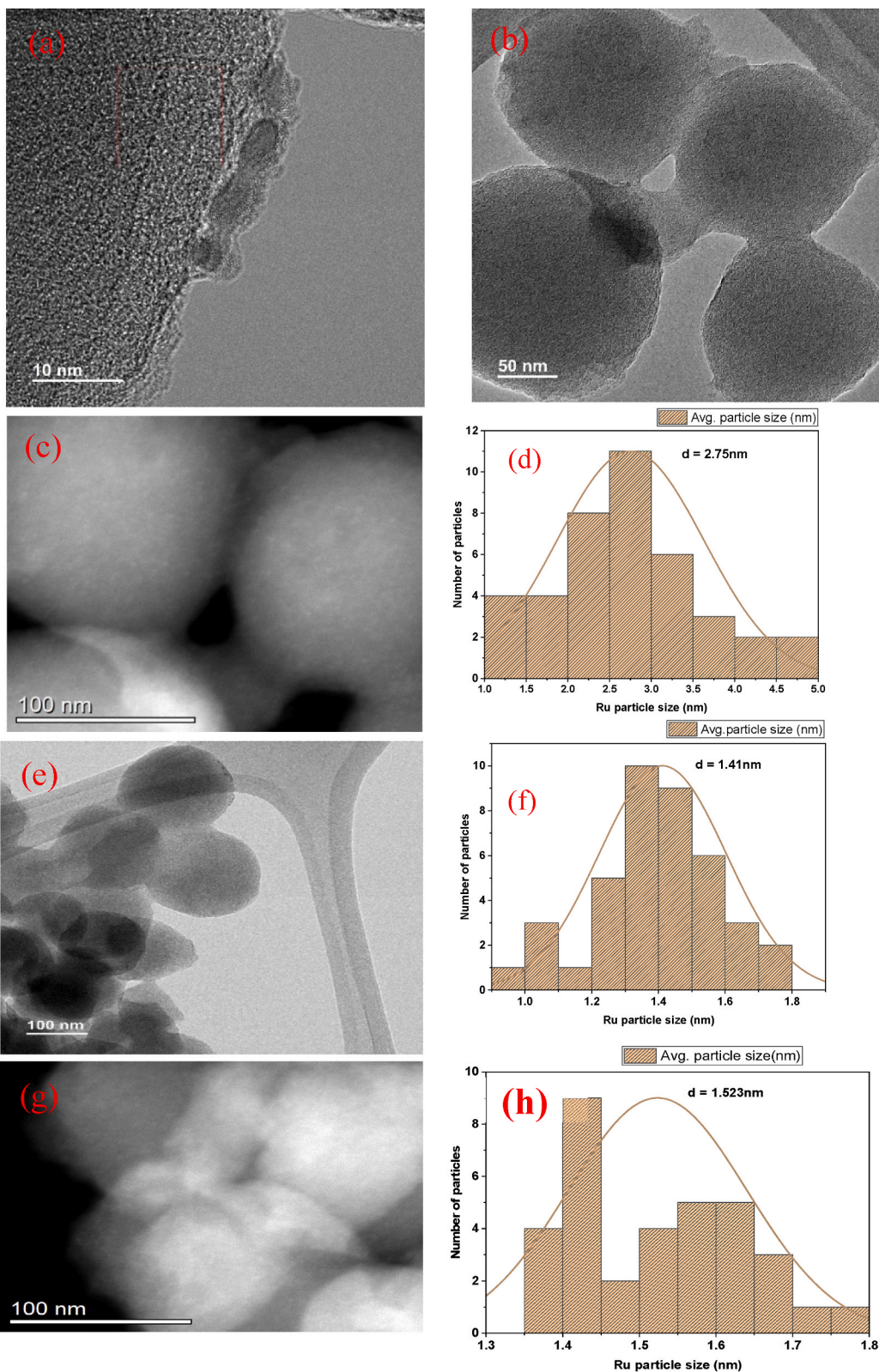


Fig. 5. TEM images of CMK-1 (a), N-CMK-1 (b), 2%Ru-CMK-1 (c), 2%Ru-N-CMK-1 (e), and 2%Ru-N-CMK-1 (Reused) (g) and their corresponding Ru NPs size distribution (d, f, h).

Table 2
Calculated values of Ru metal dispersion over different carbon supports.

Catalysts	D, Ru metal dispersion (%)
CMK-1	ND
2%Ru/CMK-1	48.65
N-CMK-1	ND
2%Ru/N-CMK-1	94.57
2%Ru/N-CMK-1 (Reused)	87.56

nitrogen moieties present in carbon nanofibers favor strong interaction with Ru metallic NPs, which consequently results in a smaller size of Ru NPs along with their homogenous distribution [70]. Thus, higher Ru metal uptake can be achieved as a result of strong interaction between nitrogen moiety and Ru metallic NPs compared to nitrogen-free carbon nanofibers. It was also revealed from the experimental investigation that, on nitrogen-doped carbon nanofibers, the percentage of Ru metallic NPs in the metallic state (i.e., zero oxidation state) was considerably higher than for nitrogen-free carbon supports [70]. In the present investigation, nitrogen functional groups on the mesoporous carbon supports played a crucial role in stabilizing the Ru metallic NPs by confining them into small sizes, inhibiting their reoxidation and thus, effectively prevent them from aggregation and held the formed ruthenium NPs on the anchoring site. These multipurpose combined features inherited by nitrogen functionalized mesoporous carbon Ru decorated metallic NPs may significantly influence the catalytic performance.

To further confirm the presence of nitrogen atoms in the carbon support and catalyst, elemental analysis (CNOH) was carried out and the result is shown in Table S1. The result shows the composition of nitrogen atoms in the carbon framework is related directly to the degree of oxygen functionality and the mass ratio of carbon to urea. It can be seen that oxygen unmodified carbon has shown a very small nitrogen. As the mass ratio of carbon to urea is increasing, the level of nitrogen atom was also increased which reveals the importance of urea in controlling the amount of nitrogen in carbon material.

As indicated in Fig. 6a, having advanced textural properties, 3D cubic-shaped morphology, and rich nitrogen functionality, the synthesized catalytic materials are remarkable for investigating CO₂ adsorption performance. Evaluated at 273 K and 1 bar condition, compared to the pristine-CMK-1 counterpart (2.51 mmol g⁻¹), N-CMK-1 has shown improved CO₂ adsorption capacity (4.00 mmol g⁻¹). This suggests the presence of high charge density at the nitrogen site on N-CMK-1, consequently responsible for the excellent adsorption capacity of CO₂ due to the enhancement of the polarizable CO₂ molecules via dipole-quadrupole interaction [71]. It is noteworthy that after 2%Ru loading, the CO₂ uptake for pristine carbon material has elevated from 2.51 to 3.35 mmol g⁻¹, which might be related to the strong affinity of Ru NPs for CO₂ adsorption [72–74]. However, the uptake capacity of 2%Ru–N-CMK-1 was reduced compared to N-CMK-1, implying the presence of a competitive adsorption site between metallic Ru NPs and nitrogen moiety which might unfavour the adsorption process. This clearly demonstrates that; the CO₂ uptake capacity of carbon materials is strongly influenced by its surface chemistry such as the presence of different functionalities of nitrogen groups. Moreover, to investigate the effect of textural properties such as BET surface area and pore volume on CO₂ uptake capacity, the surface area BET normalized was taken into consideration as shown in Fig. 6b. The result demonstrated that the textural properties of the catalyst seems insignificant influence on the adsorption capacity of the CO₂ as the materials with negligible nitrogen content, but with high BET surface area and high total pore volume, (i., CMK-1: 1890 m²g⁻¹ and 1.1124 cm³g⁻¹) possess poor gas adsorption capacity (1.36 μmol m⁻²) compared to the material with both low BET surface area and pore volume, but with high nitrogen content (i.e., N-CMK-1: 1453 m² g⁻¹ and 0.882 cm³ g⁻¹) that adsorb CO₂ to approx. 2.7 μmol m⁻² capacity. A similar observation was seen with 2%Ru–N-CMK-1 which uptake CO₂ to approx. 2.65 μmol m⁻². It can therefore be concluded from the overall results that the combination of textural features and suitable

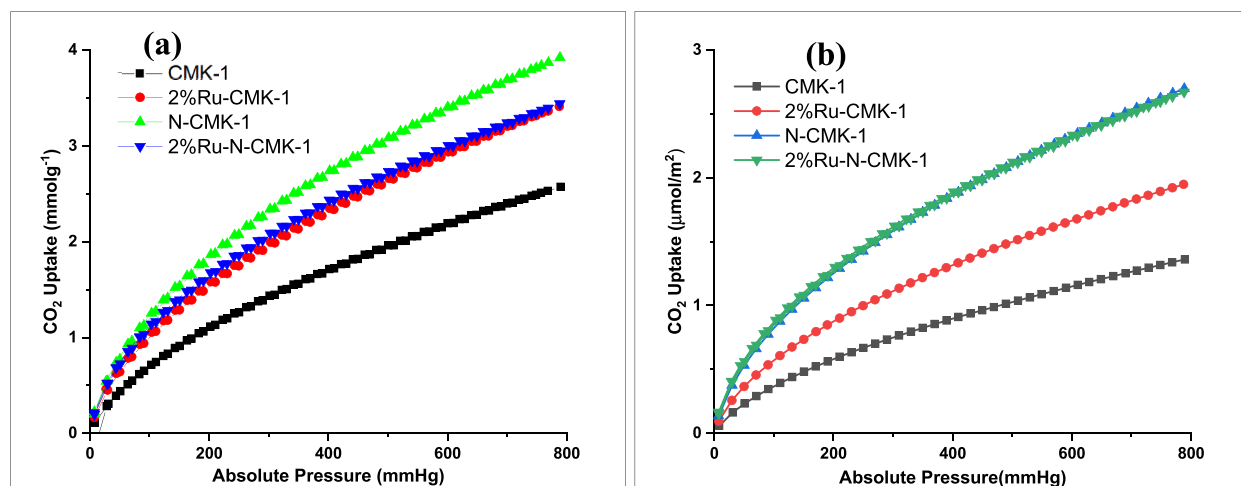
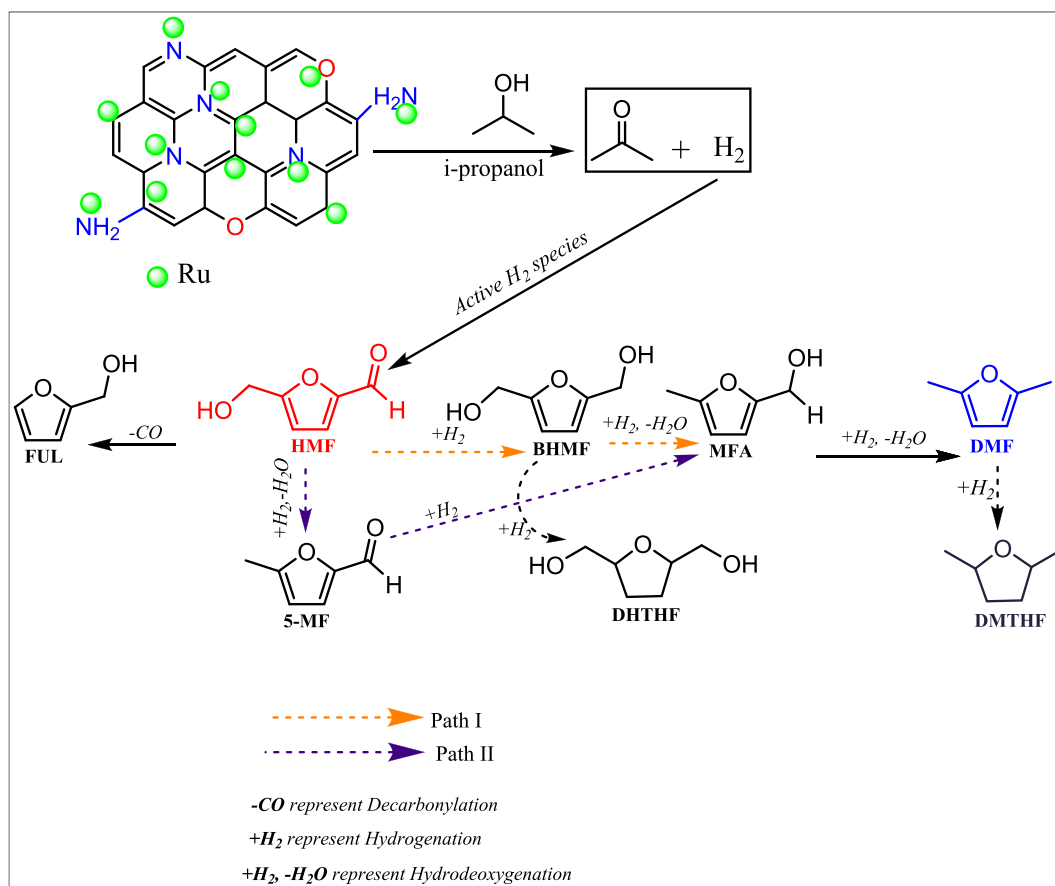


Fig. 6. CO₂ Sorption isotherms (a) and Surface area BET normalized (b) at 273 K for pristine CMK-1, 2%Ru-CMK-1, N-CMK-1 and 2%Ru–N-CMK-1.

nitrogen functionality on carbon materials contributes to a positive effect on CO₂ uptake capacity than the effect of single textural properties. A similar phenomenon was previously reported in the literature [75,76].

3.1. Evaluation of catalytic performance

The reaction networks for the CTH of HMF to DMF is shown in Scheme 1. Subsequently, the performance of freshly reduced catalysts with and without nitrogen contents are shown in Table 4. The blank test shows no activity toward the conversion of HMF and product yield, indicating clearly that the presence of a catalyst was essential for this reaction (Table 3, entry 1) and Fig. S2(a). With 2% Ru-CMK-1, a complete HMF conversion was achieved, even though the yield of DMF is as low as 30.6% (Table 3, entry 2) and Fig. S1(a). Increasing ruthenium loading to 5% resulted in low catalytic performance in terms of HMF conversion (80.50 %) and DMF yield, 22.4% (Table 3, entry 3). This might be due to the aggregations of Ru metallic NPs due to excess metal loading. In contrast, DMF yield remarkably rose to a higher value with nitrogen-modified carbon support, with HMF conversion attained at 100%. Notably, as high as 88.0% DMF yield was obtained with 2%Ru-N-CMK-1 (Table 3, entry 4), and see also Figs. S1(b) and S2(b). It is interesting to note that, with 5%Ru-N-CMK-1 the performance of the catalyst rose in terms of HMF conversion (100%) and DMF yield (60.93%) compared to undoped, signifying the importance of nitrogen functionality on the activity of the catalysts (Table 3, entry 5). These results clearly show that the Lewis basicity [77] inherited by nitrogen functionalities plays a vital role in the dehydrogenation of *i*-propanol, where the adsorbed hydrogen species during the CTH can immediately hydrogenate HMF adsorbed on Ru metallic NPs. To verify this phenomenon, we demonstrated three additional separate tests: 1) The hydrogenolysis of HMF was conducted at 8 bar of H₂ pressure (a total H₂ partial pressure of 8 bar was developed during the CTH reaction at 160 °C over 2% Ru-N-CMK-1 with *i*-Propanol) using acetone as a solvent (Table 3, entry 6). Even though HMF was fully converted, no DMF was formed. This demonstrates that the hydrogenation of HMF using a hydrogen donor via CTH could be more efficient than that utilizing external H₂ hydrogen and that the CTH reaction could occur through metal hydride route. 2) In order to further explore the origin of the catalytic activity, *i*-propanol dehydrogenation ability of different catalysts was investigated and shown in Fig. 8b. In the absence of HMF, the yield of acetone decreases in the following order: 2%Ru-N-CMK-1 > N-CMK-1 > 2%Ru-CMK-1 > CMK-1 not however well consistent with the amount of



Scheme 1. Schematic of reaction pathway for CTH of HMF into DMF in *i*-propanol over 2%Ru-N-CMK-1.

Notation: HMF; 5-hydroxymethylfurfural, FUL; Furfuryl alcohol, MFA; 2-methylfuran, 5-MF; 5-methylfurfural, BHMF; 2,5-bishydroxymethylfuran, DMF; 2,5-dimethylfuran, DHTHF; 2,5-dihydroxytetrahydrofuran, DMTHF; 2,5-dimethyltetrahydrofuran.

Table 3
Product distribution of HMF hydrogenation over different catalysts.

Entry	Catalysts	HMF Conv. (mol%)	Product Yield (mol %)							
			DMTHF	DMF	FUL	MFA	5-MF	BHTHF	BHMF	other
1	Blank	0	0	0	0	0	0	0	0	0
2	2%Ru-CMK-1	100	0	30.59	0.85	2.16	8.54	0	27.73	30.13
3	2%Ru-N-CMK-1 ^a	100	0	88.0	1.92	0.58	0	0	9.34	0.24
4	5%Ru-CMK-1	80.50	0	22.40	0	0.5	15.36	0	0	42.24
5	5%Ru-N-CMK-1 ^a	100	0	60.93	2.37	1.20	1.1	0.81	0	33.59
6	2%Ru-N-CMK-1 ^{a,*}	100	0	0	0	0	0	0	99.04	0.96

Reaction condition: Temperature = 160 °C, Time = 8 h, P_{N₂} = 20 bar, stirring speed = 400 rpm, [HMF] = 20 mM, Reaction volume = 4 mL, Catalyst weight = 10 mg *8 bar H₂ pressure was used with Acetone (4 mL) as a solvent instead of *i*-Propanol.

^a Contains a 5.5 wt% Nitrogen.

Table 4
Controlled experiments for the production of DMF from hydrogenolysis of intermediates via CTH.^a

Entry	Substrates	Substrate conversion (% mol)	Products Yield (%mol)	
			DMF	MFA
1	BHMF	67.3	46.7	15.6
2	5-MF	87.4	84.4	ND

^a Reaction conditions: Temperature = 160 °C, Time = 8 h, Reaction volume = 4 mL; [BHMF, 5-MF] = 20 mM, Catalyst weight = 10 mg, P_{N₂} = 20 bar.

order of the basic strength. This result strongly proves that for the effective dehydrogenation of *i*-propanol to H₂ and acetone, compared to the basic surface site alone, the synergistic effect of ruthenium and basic site density leads to high catalytic activity in CTH of HMF to DMF. Therefore, it can reasonably be concluded that the surface cooperation between the ruthenium surface area and base site is responsible for high activity of 2%Ru-N-CMK-1.3) To further confirm the role of Lewis base on 2%Ru-N-CMK-1 for dehydrogenation of *i*-propanol and subsequent CTH of HMF, benzoic acid was added to a reaction system to perform a poisoning experiment (Table S3). When the basic site of 2%Ru-N-CMK-1 was poisoned by benzoic acid, the conversion of HMF and yield of DMF decreased remarkably to 50% and 34% respectively. The result witness the heavily dependence of DMF synthesis from HMF via CTH on the Lewis basic site of 2%Ru-N-CMK-1. To delineate the mechanism for the hydrogenolysis of HMF to DMF using *i*-propanol as the hydrogen donor, however, further studies are required.

The influence of reaction temperature on the CTH of HMF to DMF over 2%Ru-N-CMK-1 was investigated (Fig. 7a). It is interesting that even at a low temperature (100 °C), the conversion of HMF is maintained above 80%. As the reaction temperature rose from 100 to 160 °C, the DMF formation increased linearly and the maximum DMF yield reached a high value of 88% at 160 °C. This demonstrates the temperature-dependent DMF formation pathway. However, a reduction in the DMF yield was vividly observed when the reaction temperature was raised to 180 °C. At this high temperature, no over-hydrogenation product of DMF; dimethyl tetrahydrofuran (DMTHF) was seen, which is different from the previous report [78]. Probably too high reaction temperature may induce the cracking of HMF furan ring to gaseous molecules such as CH₄ and C₂H₆, so might affect the progress of the hydrodeoxygenation process and cause the reduction of DMF yield. It was reported in the previous research that HMF is prone to coking if reacted at high temperature ≥180 °C [33].

The time effect of hydrodeoxygenation (HDO) of HMF to DMF via CTH over 2%Ru-N-CMK-1 was investigated and represented in Fig. 7b. With increasing reaction time, the conversion of HMF was increased and complete conversion was achieved at 8 h. The intermediate products (5-MF and BHMF) were further converted to DMF as the time continuously rose to 8 h, though the conversion of HMF remained basically unchanged after 8 h. The yield of DMF was increased continuously with increasing reaction time and reached a maximum of 88% at 8 h and then decreased for tested reaction time beyond 8 h. This might be attributed to the cracking of the furan ring and the formation of the coke on the surface of the catalyst at the current experimental temperature and prolonged reaction time, which is not conducive to the formation of DMF.

Furthermore, for the CTH of HMF into DMF over 2%Ru-N-CMK-1, the effect of various hydrogen donors was studied and depicted in Fig. 7c. Obviously, HMF conversion was lower than 80% and DMF yield was less than 58% when methanol, ethanol, *n*-propanol, and *n*-butanol were used as a hydrogen source. However, HMF conversion and DMF yield exceeded 95% and 67% when hydrogen donors were switched respectively to *i*-propanol and *s*-butanol, suggesting a higher activity of secondary alcohols than primary alcohols for the selective synthesis of DMF from HMF via CTH. The higher activity of secondary alcohols for this particular reaction might be attributed to their lower reduction potentials (RPs), where RPs specifically represent the differential of standard molar formation enthalpies between alcohols and their relevant carbonyl products [79].

The lower RPs of secondary alcohols mean a higher tendency to release a hydrogen atom; making it easy to eliminate β-H from secondary alcohols, hence can promote the selective synthesis of DMF from HMF [80]. Furthermore, another important factor that can excel in the activity of secondary alcohols for CTH is their steric hindrances (SHs) [81]. As can be seen from Table S2, a higher HMF conversion and DMF yield was achieved with *i*-Propanol (solvent with relatively higher RP) compared with *s*-butanol, and the same

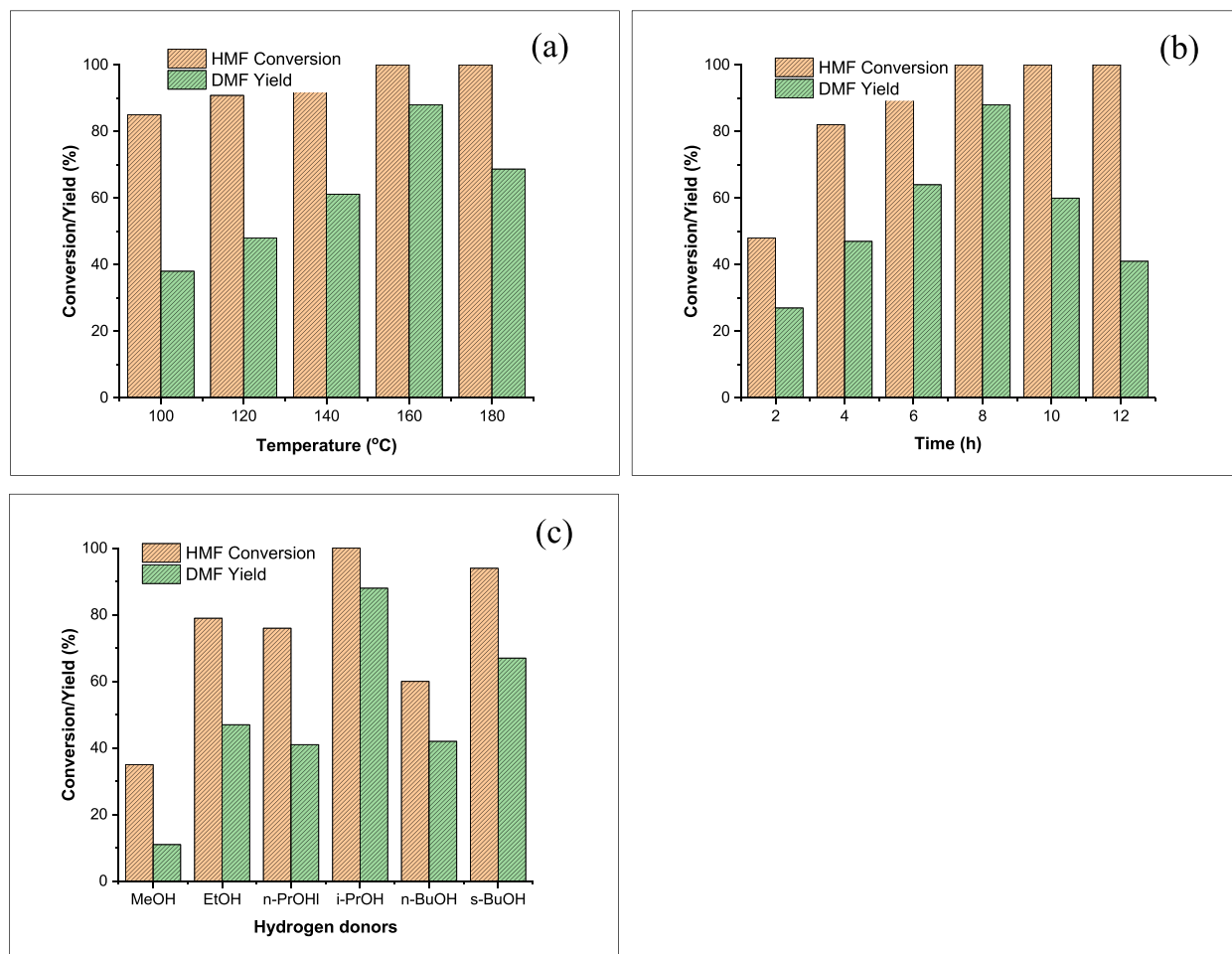


Fig. 7. Effect of reaction temperature (a) and reaction time (b) and alcohol types (c) on CTH of HMF to DMF over 2%Ru-N-CMK-1: Reaction conditions: (a)Time = 8 h, Reaction volume = 4 mL; [HMF] = 20 mM in *i*-propanol, Catalyst weight = 10 mg, P_{N_2} = 20 bar, speed = 400 rpm; (b) Temperature = 160 °C, Reaction volume = 4 mL; [HMF] = 20 mM in *i*-propanol, Catalyst weight = 10 mg, P_{N_2} = 20 bar, speed = 400 rpm; (c) Time = 8 h, Reaction volume = 4 mL; [HMF] = 20 mM in alcohols, Catalyst weight = 10 mg, P_{N_2} = 20 bar, temperature = 160 °C, speed = 400 rpm.

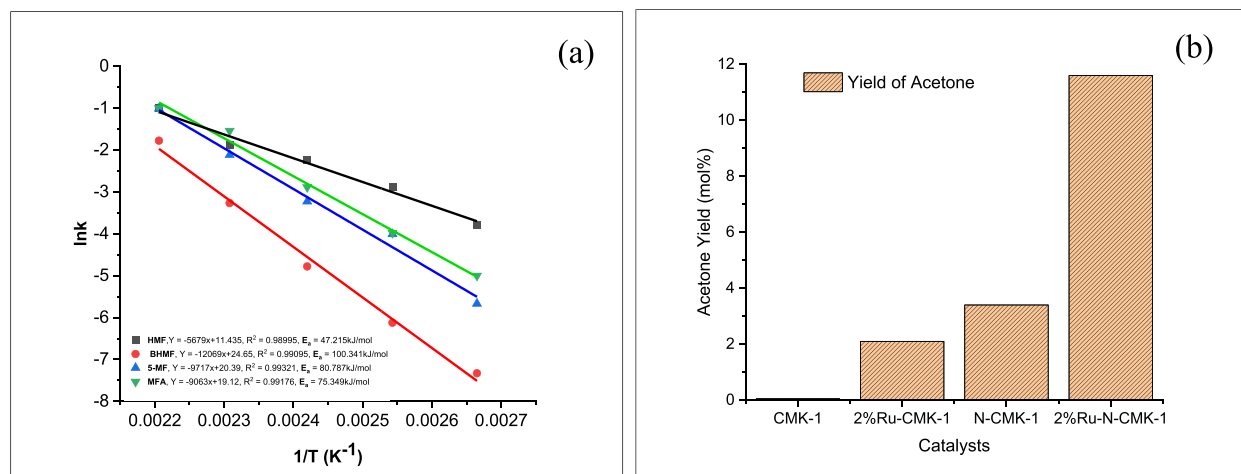


Fig. 8. Profiles of Arrhenius plot of HMF and different intermediates in the selective hydrogenolysis of HMF via CTH over 2%Ru-N-CMK-1 catalyst (a) and change in the yield of acetone in different catalyst (b) at Reaction conditions: Time = 8 h, Reaction volume = 4 mL; [*i*-Propanol] = 20 mM, Catalyst weight = 10 mg, P_{N_2} = 20 bar, Temperature = 160 °C, speed = 400 rpm.

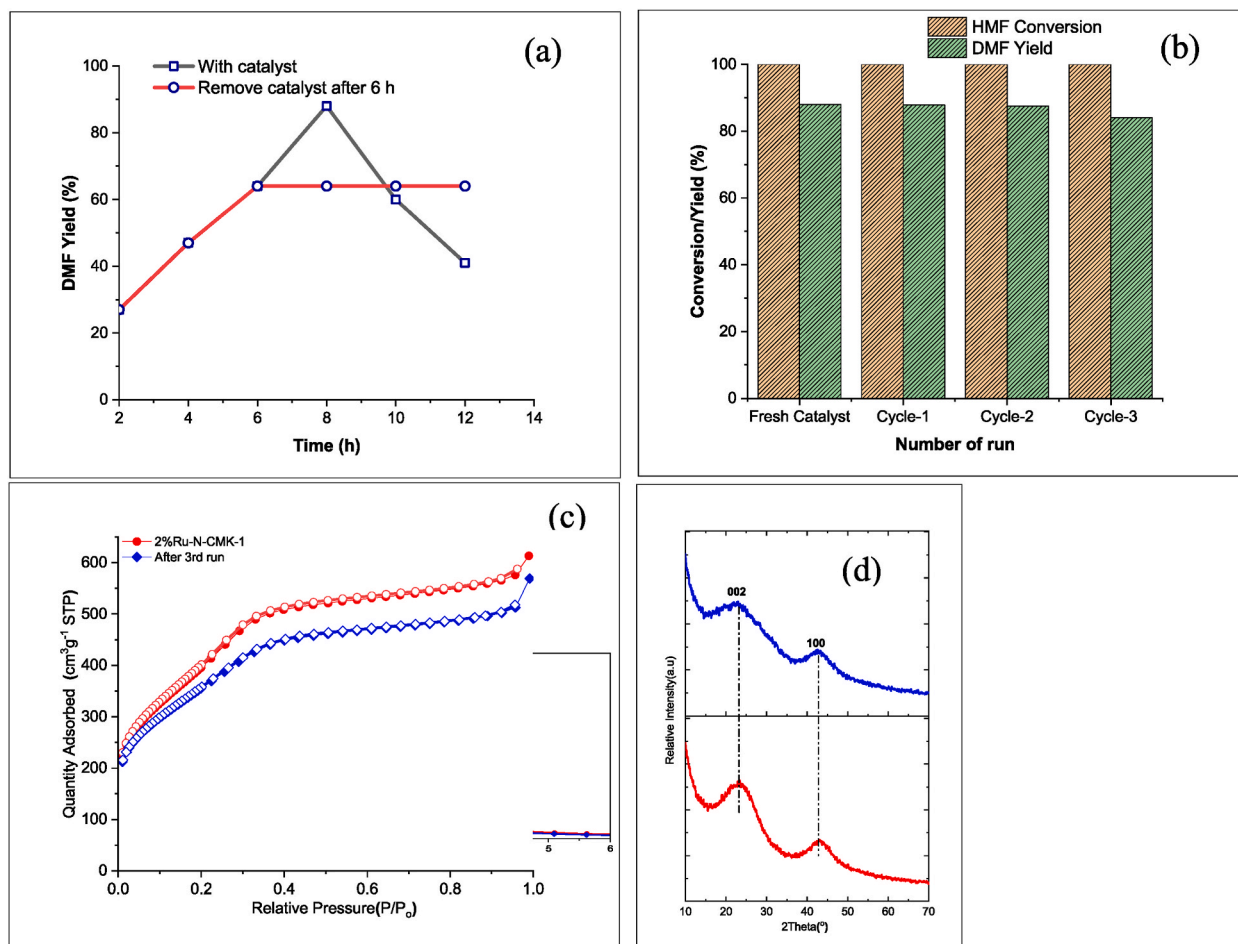


Fig. 9. Heterogeneity (a), recyclability (b), N₂-sorption isotherm (c), and XRD pattern (d) of fresh and spent 2%Ru-N-CMK-1 catalyst [b-d].

situation was also observed in ethanol and *n*-*n*-butanol.

This activity difference is mainly due to the smaller SHs of *i*-propanol and ethanol than *s*-butanol and *n*-butanol respectively. In a nutshell, alcohols with smaller SHs are too conductive for diffusion over the surface and in the internal channel of the catalyst, thus further promoting the selective conversion of HMF into DMF via CTH route. Thus, it can be assured that for the selective synthesis of DMF from HMF, secondary alcohols with low reduction potentials and low steric hindrances are perfect hydrogen donors in the presence of 2% Ru loaded on a nitrogen-doped ordered mesoporous carbon catalyst. Based on these facts, HMF could be entirely converted with 88% DMF yield with the optimum condition of temperature, time, and hydrogen donor to be set respectively at 160 °C, 8 h, and *i*-propanol; which was higher than those in many previous reports (Table S4).

3.2. Investigation of the reaction pathway

Generally, two distinct pathways are followed for the formation of DMF from HMF (Scheme 1) with hydrogenation and hydrogenolysis of alcohol and carbonyl group preceding via intermediate 5-MF or another intermediate BHMF [82]. Here, two controlled experiments were carried out using BHMF and 5-MF as reaction intermediates feedstock to corroborate our hypothesis and explore the reaction pathway over a 2%Ru-N-CMK-1 catalyst (Table 4).

It was clear that DMF was produced from both substrates. More than 87% of 5-MF was transformed into DMF without the detection of MFA when 5-MF was used as a substrate. On the contrary, employing BHMF as a substrate resulted in the detections of 46.7% and 15.6% yield respectively in DMF and MFA.

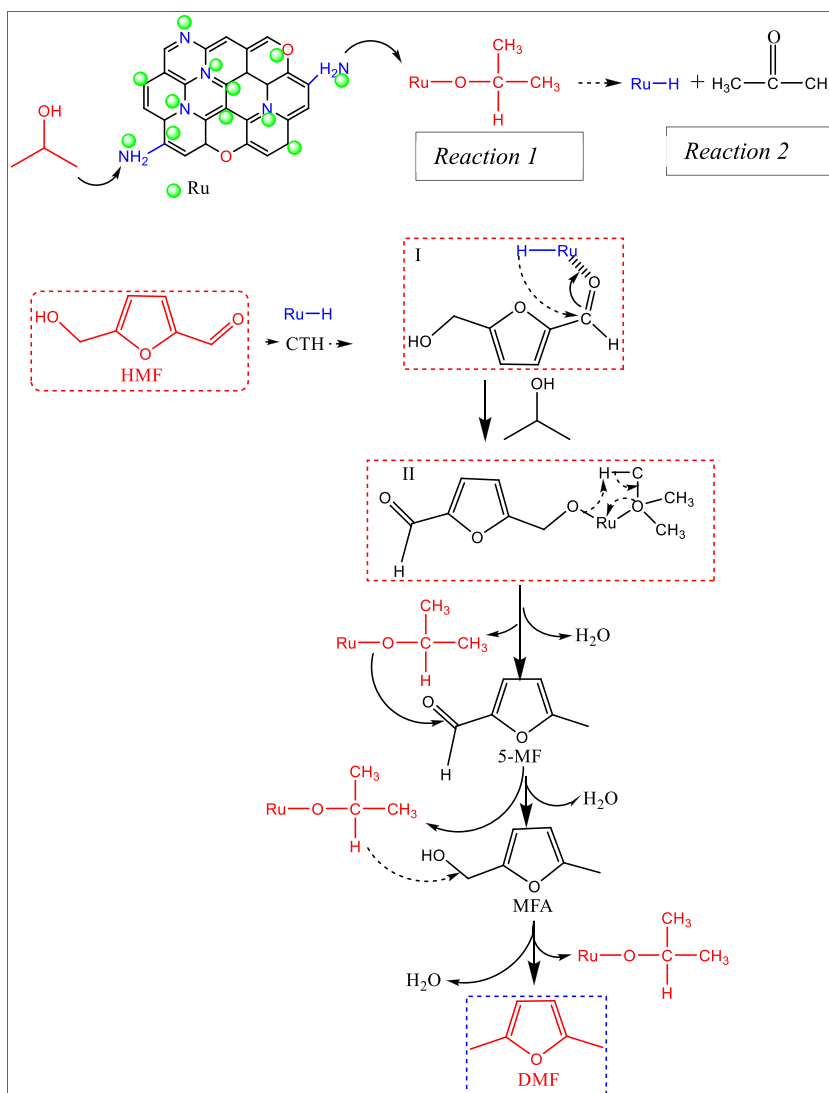
Therefore, it can be assured that HDO of HMF to DMF via CTH proceed through path II of 5-MF intermediate rather than path I of BHMF intermediate (Scheme 1). Hence it can be inferred that the hydroxyl group in HMF could first hydrodeoxygenated to form a 5-MF intermediate and a further hydrodeoxygenation process was followed to form DMF. Our current finding is in agreement with the previous report that emphasized on HDO of HMF to DMF via 4 MPa H₂ pressure as a reductant over 5% Cu–15% Ni/BC catalyst [33].

Generally, a pseudo-first-order reaction is considered during the HDO process of biomass [33] and the Arrhenius formula was adopted to calculate the activation energy (E_a) of the HMF and intermediates as shown in Fig. 8a. It can be observed that the E_a of HMF

conversion is 47.215 kJ/mol. This is significantly lower than the E_a of HMF conversion over nickel-supported mesoporous carbon which was found to be 205.1 kJ/mol [83]. Thus, the present study confirms the effectiveness of 2%Ru–N-CMK-1 catalyst for the selective formation of DMF from HMF via CTH route in *i*-propanol. Furthermore, it was observed that 5-MF possesses a lower value of E_a (80.787 kJ/mol) compared to that of BHMF (E_a ; 100.341 kJ/mol), manifesting the rate of reaction from HMF to 5-MF is faster than that from HMF to BHMF. Consequently, during CTH of HMF, 5-MF is more likely to occur than BHMF further confirming that 5-MF facilitates the formation of DMF in this reaction. The intermediate MFA conversion shows the lowest E_a of 75.349 kJ/mol indicated that the rate determined step is the first hydroxyl group hydrogenolysis during the HDO process of DMF formation.

3.3. Proposed reaction mechanism

From the experimental demonstration and reaction pathway validated by Arrhenius reaction kinetics, the reaction mechanism for CTH of HMF to DMF can be proposed as shown in Scheme 2. The proposed reaction mechanism would involve several main steps: First, the ruthenium hydride has formed due to the activation of *i*-propanol with ruthenium as shown in reaction 1. Second, the breakdown of generated ruthenium hydride to Ru–H and acetone (reaction 2). Third, the formation of transition complexes I from the reaction of Ru–H with the carbonyl group of HMF. Fourth, the reaction between the generated transition complex I and hydrogen donor via a five-membered ring transition state will attack HMF carbonyl carbon and subsequently, the transition complex II is formed. Fifth, 5-MF will be generated as an objective product through the elimination of ruthenium hydride which will participate in subsequent catalytic events. Moreover, 5-MF will be hydro-deoxygenated to MFA through the elimination of ruthenium hydride and H₂O. Eventually, the



Scheme 2. Proposed reaction mechanism for CTH of HMF into DMF in *i*-propanol over 2%Ru–N-CMK-1.

eliminated ruthenium hydride will attack the hydroxyl group of MFA and a high yield of DMF will be achieved via CTH through elimination of water.

3.4. Catalytic stability of 2%Ru–N-CMK-1

One of the great advantages of heterogenous catalysts over homogenous ones is their recyclability. In this study, the solid catalyst was removed by filtration from the reaction mixture after 6 h at 160 °C to prove its heterogeneity. Subsequently, the supernatant was allowed to react for another 6 h and no further reaction was found in the absence of 2%Ru–N-CMK-1, as can be seen from Fig. 9a. The DMF yield was maintained at 62.5% and shows no increment. The leachability of Ru in the supernatant was also checked by ICP-AES and Ru leaching into the solution was not detected, thus is a clear indication of the heterogeneous nature of this catalyst (Table 1). The recyclability study was also performed on the most effective catalyst: 2%Ru–N-CMK-1 (Fig. 9b). Before the evaluation of recyclability, the catalyst was separated from the reaction mixture, washed thoroughly with 40 mL of *i*-propanol, oven-dried at 95 °C for 3 h. The result demonstrated that the activity of the catalysts in terms of HMF conversion and DMF yield remains the same for three reaction cycles, indicating that 2%Ru–N-CMK-1 possessed an excellent stability. Meanwhile, the spent catalyst after the third reaction cycle was analyzed by N₂-sorption isotherm (Fig. 9c), small angle XRD (Fig. 9d), TEM (Fig. 5 g,h) and the characterization results show a negligible significant change between fresh and reused catalyst in terms of morphology, size, structure and nitrogen content, further proving utmost stability of 2%Ru–N-CMK-1 in *i*-propanol for the formation of DMF from HMF via CTH reaction.

4. Conclusion

In this work, we have synthesized a mesoporous support material where the active catalytic metallic nanoparticle was dispersed. A mesoporous silica nanoparticle (MCM-48) was first synthesized by soft templating approach and subsequently, owing to its 3D – cubic pore shape, high BET surface area, and high pore volume, a mesoporous carbon nanoparticle; (CMK-1) was synthesized via hard templating of pre-synthesized MCM-48. The surface chemistry of the support was modified via doping with nitrogen by a simple hydrothermal method using urea as a chemical dopant and reducing agent. The successful synthesis of the supports was characterized by different techniques. A ruthenium metallic nanoparticle was dispersed over nitrogen-doped carbon support and the evaluation of the catalytic performance shows that HMF could be completely converted with 88% DMF yield by CTH using *i*-Propanol as a hydrogen donor. The catalyst was recycled and reused three times without significant loss in activity. As revealed from a series of characterization techniques and experimental results, the incorporation of nitrogen atoms in the carbon framework brought a basic surface site and improved Ru species dispersion was mainly the reason for improvement of the catalytic performance. Correspondingly, the cooperative governance between the surface basic sites and Ru species are a key factor in the dehydrogenation of *i*-propanol and hydrogenolysis of HMF. Moreover, the enhancement in the stability of the catalyst was inherited mainly from the strong interaction between the Ru species and the support that could suppress the aggregation of Ru NPs. So, for future catalyst design in the field of biomass conversion, the attractive feature of the present Ru-based catalyst could provide a guiding principle.

Data availability statement

Data included in article/supplementary material/referenced in article.

CRediT authorship contribution statement

Jibril Goli Buta: Writing – review & editing, Writing – original draft, Visualization, Validation, Supervision, Project administration, Methodology, Investigation, Formal analysis, Data curation, Conceptualization. **Bayisa Dame:** Writing – review & editing. **Tariku Ayala:** Writing – review & editing.

Declaration of competing interest

The authors declare that they have no known competing financial interests or personal relationships that could have appeared to influence the work reported in this paper.

Acknowledgment

The authors gratefully acknowledge Adama Science and Technology University (ASTU) for financial support.

Appendix A. Supplementary data

Supplementary data to this article can be found online at <https://doi.org/10.1016/j.heliyon.2024.e26690>.

References

- [1] L. Hu, et al., Recent advances in catalytic transformation of biomass-derived 5-hydroxymethylfurfural into the innovative fuels and chemicals, *Renew. Sustain. Energy Rev.* 74 (2017) 230–257.
- [2] C. Aellig, I. Hermans, Continuous D-Fructose dehydration to 5-hydroxymethylfurfural under mild conditions, *ChemSusChem* 5 (9) (2012) 1737–1742.
- [3] D. Scholz, C. Aellig, I. Hermans, Catalytic transfer hydrogenation/hydrogenolysis for reductive upgrading of furfural and 5-(hydroxymethyl)furfural, *ChemSusChem* 7 (1) (2014) 268–275.
- [4] S. Zhong, et al., Combustion and emissions of 2,5-dimethylfuran in a direct-injection spark-ignition engine, *Energy Fuels* 24 (5) (2010) 2891–2899.
- [5] P. Mäki-Arvela, D. Ruiz, D.Y. Murzin, Catalytic hydrogenation/hydrogenolysis of 5-hydroxymethylfurfural to 2,5-dimethylfuran, *ChemSusChem* 14 (1) (2021) 150–168.
- [6] T.S. Hansen, et al., One-pot reduction of 5-hydroxymethylfurfural via hydrogen transfer from supercritical methanol, *Green Chem.* 14 (9) (2012) 2457–2461.
- [7] D. Dhana Lakshmi, et al., Selective hydrodeoxygenation of 5-hydroxymethylfurfural to 2, 5-dimethylfuran over mesoporous silica supported copper catalysts, *Mater. Sci. Energy Technol.* 4 (2021) 357–366.
- [8] H. Xia, J. Li, M. Zhou, Advances in selective hydrogenation of 5-hydroxymethylfurfural over heterogeneous metal catalysts, *Energies* 16 (2023), <https://doi.org/10.3390/en16196793>.
- [9] J. Luo, et al., Mechanisms for high selectivity in the hydrodeoxygenation of 5-hydroxymethylfurfural over PtCo nanocrystals, *ACS Catal.* 6 (7) (2016) 4095–4104.
- [10] T. Gan, et al., Facile synthesis of kilogram-scale Co-alloyed Pt single-atom catalysts via ball milling for hydrodeoxygenation of 5-hydroxymethylfurfural, *ACS Sustain. Chem. Eng.* 8 (23) (2020) 8692–8699.
- [11] Xia, J., et al., Hydrogenolysis of 5-Hydroxymethylfurfural to 2,5-Dimethylfuran over a Modified CoAl-Hydroxalcalite Catalyst (2296-2646 (Print)).
- [12] J. Xia, et al., Hydrogenolysis of 5-hydroxymethylfurfural to 2,5-dimethylfuran over a modified CoAl-hydroxalcalite catalyst, *Front. Chem.* 10 (2022).
- [13] X. Wang, Y. Liu, X. Liang, Hydrogenolysis of 5-hydroxymethylfurfural to 2,5-dimethylfuran over supported Pt-Co bimetallic catalysts under mild conditions, *Green Chem.* 20 (12) (2018) 2894–2902.
- [14] Y. Zu, et al., Efficient production of the liquid fuel 2,5-dimethylfuran from 5-hydroxymethylfurfural over Ru/Co3O4 catalyst, *Appl. Catal. B Environ.* 146 (2014) 244–248.
- [15] J. Zhang, K. Dong, W. Luo, PdCl2-catalyzed hydrodeoxygenation of 5-hydroxymethylfurfural into 2,5-dimethylfuran at room-temperature using polymethylhydrosiloxane as the hydrogen donor, *Chem. Eng. Sci.* 201 (2019) 467–474.
- [16] Y. Li, et al., Hydrogenation and hydrogenolysis of 5-hydroxymethylfurfural to 2,5-dimethylfuran via synergistic catalysis of Ni2In and acid-base sites, *Appl. Surf. Sci.* 604 (2022) 154579.
- [17] W. Han, et al., Efficient conversion of 5-hydroxymethylfurfural to 2,5-dimethylfuran by the rational design of NiZn catalysts, *Mol. Catal.* 531 (2022) 112698.
- [18] C. Castillo, et al., Recent advances in catalytic conversion of 5-hydroxymethylfurfural (5-HMF) to 2,5-dimethylfuran (2,5-DMF): mechanistic insights and optimization strategies, *ChemCatChem* 15 (15) (2023) e202300480.
- [19] D. Guo, et al., Titanium silicalite-1 supported bimetallic catalysts for selective hydrogenolysis of 5-hydroxymethylfurfural to biofuel 2, 5-dimethylfuran, *Chem. Eng. J. Adv.* 5 (2021) 100081.
- [20] Y. Li, et al., Functional carbon-supported nanocatalysts for biomass conversion, *Mol. Catal.* 538 (2023) 113003.
- [21] W. Zhao, et al., Cu-Co nanoparticles supported on nitrogen-doped carbon: an efficient catalyst for hydrogenation of 5-hydroxymethylfurfural into 2,5-bis(hydroxymethyl)furan, *Mol. Catal.* 524 (2022) 112304.
- [22] W. Zhao, et al., Highly efficient syntheses of 2,5-bis(hydroxymethyl)furan and 2,5-dimethylfuran via the hydrogenation of biomass-derived 5-hydroxymethylfurfural over a nickel-cobalt bimetallic catalyst, *Appl. Surf. Sci.* 577 (2022) 151869.
- [23] D. Guo, et al., Selective hydrogenolysis of 5-hydroxymethylfurfural to produce biofuel 2, 5-dimethylfuran over Ni/ZSM-5 catalysts, *Fuel* 274 (2020) 117853.
- [24] Z. Zeng, et al., Highly selective production of the biofuel 2,5-dimethylfuran from 5-hydroxymethylfurfural over Co/N-C catalysts, *React. Chem. Eng.* 8 (2) (2023) 455–464.
- [25] D. Rodríguez-Padrón, et al., Tuning the selectivity of the hydrogenation/hydrogenolysis of 5-hydroxymethylfurfural under batch multiphase and continuous-flow conditions, *ChemSusChem* 15 (13) (2022) e202200503.
- [26] G.-H. Wang, et al., Platinum-cobalt bimetallic nanoparticles in hollow carbon nanospheres for hydrogenolysis of 5-hydroxymethylfurfural, *Nat. Mater.* 13 (3) (2014) 293–300.
- [27] J. Mitra, X. Zhou, T. Rauchfuss, Pd/C-catalyzed reactions of HMF: decarbonylation, hydrogenation, and hydrogenolysis, *Green Chem.* 17 (1) (2015) 307–313.
- [28] X. Wang, et al., Catalytic hydrogenolysis of biomass-derived 5-hydroxymethylfurfural to biofuel 2, 5-dimethylfuran, *Appl. Catal. Gen.* 576 (2019) 85–95.
- [29] B.S. Solanki, C.V. Rode, Selective hydrogenolysis of 5-(hydroxymethyl)furfural over Pd/C catalyst to 2,5-dimethylfuran, *J. Saudi Chem. Soc.* 23 (4) (2019) 439–451.
- [30] M. Besson, P. Gallezot, C. Pinel, Conversion of biomass into chemicals over metal catalysts, *Chem. Rev.* 114 (3) (2014) 1827–1870.
- [31] Y. Wang, et al., A magnetic CoRu-CoOx nanocomposite efficiently hydrogenates furfural to furfuryl alcohol at ambient H2 pressure in water, *Chem. Commun.* 56 (26) (2020) 3765–3768.
- [32] A.S. Nagpure, N. Lucas, S.V. Chilukuri, Efficient preparation of liquid fuel 2,5-dimethylfuran from biomass-derived 5-hydroxymethylfurfural over Ru-NaY catalyst, *ACS Sustain. Chem. Eng.* 3 (11) (2015) 2909–2916.
- [33] C. Zhu, et al., Selective hydrodeoxygenation of 5-hydroxymethylfurfural to 2,5-dimethylfuran over alloyed Cu-Ni encapsulated in biochar catalysts, *ACS Sustain. Chem. Eng.* 7 (24) (2019) 19556–19569.
- [34] Y. Wang, et al., Efficient hydrogenation of 5-hydroxymethylfurfural using a synergistically bimetallic Ru-Ir/C catalyst, *Chem. Commun.* 57 (14) (2021) 1742–1745.
- [35] P. Priece, et al., Fast catalytic hydrogenation of 2,5-hydroxymethylfurfural to 2,5-dimethylfuran with ruthenium on carbon nanotubes, *Ind. Eng. Chem. Res.* 57 (6) (2018) 1991–2002.
- [36] S. Mhadmhan, et al., Continuous flow selective hydrogenation of 5-hydroxymethylfurfural to 2,5-dimethylfuran using highly active and stable Cu-Pd/reduced graphene oxide, *ACS Sustain. Chem. Eng.* 7 (16) (2019) 14210–14216.
- [37] R.J. Chimentão, et al., Catalytic transformation of biomass-derived 5-hydroxymethylfurfural over supported bimetallic iridium-based catalysts, *J. Phys. Chem. C* 125 (18) (2021) 9657–9678.
- [38] B. Chen, et al., Carbon-coated Cu-Co bimetallic nanoparticles as selective and recyclable catalysts for production of biofuel 2,5-dimethylfuran, *Appl. Catal. B Environ.* 200 (2017) 192–199.
- [39] P. Yang, et al., Catalytic transfer hydrogenation/hydrogenolysis of 5-hydroxymethylfurfural to 2,5-dimethylfuran over Ni-Co/C catalyst, *Fuel* 187 (2017) 159–166.
- [40] T. Thananathanachon, T.B. Rauchfuss, Efficient production of the liquid fuel 2,5-dimethylfuran from fructose using formic acid as a reagent, *Angew. Chem. Int. Ed.* 49 (37) (2010) 6616–6618.
- [41] N. Cao, et al., Selective hydrogenolysis of 5-hydroxymethylfurfural to 2,5-dimethylfuran with ethanol as a hydrogen donor over β -Mo2C embedded in carbon microspheres, *Sustain. Energy Fuels* 5 (18) (2021) 4749–4757.
- [42] Á. O'Driscoll, J.J. Leahy, T. Curtin, The influence of metal selection on catalyst activity for the liquid phase hydrogenation of furfural to furfuryl alcohol, *Catal. Today* 279 (2017) 194–201.
- [43] Y. Wang, et al., Comparative study of supported monometallic catalysts in the liquid-phase hydrogenation of furfural: batch versus continuous flow, *ACS Sustain. Chem. Eng.* 6 (8) (2018) 9831–9844.
- [44] Y. Deng, et al., Solvent tunes the selectivity of hydrogenation reaction over α -MoC catalyst, *J. Am. Chem. Soc.* 140 (43) (2018) 14481–14489.

- [45] Y. Wang, et al., Highly selective hydrogenation of phenol and derivatives over a Pd@carbon nitride catalyst in aqueous media, *J. Am. Chem. Soc.* 133 (8) (2011) 2362–2365.
- [46] P. Gogoi, et al., Controlling and stabilization of Ru nanoparticles by tuning the nitrogen content of the support for enhanced H₂ production through aqueous-phase reforming of glycerol, *ACS Catal.* 10 (4) (2020) 2489–2507.
- [47] L. Zhao, et al., Nitrogen-containing hydrothermal carbons with superior performance in supercapacitors, *Adv. Mater.* 22 (45) (2010) 5202–5206.
- [48] K. Gong, et al., Nitrogen-doped carbon nanotube arrays with high electrocatalytic activity for oxygen reduction, *Science* 323 (5915) (2009) 760.
- [49] J. Long, et al., Nitrogen-doped graphene nanosheets as metal-free catalysts for aerobic selective oxidation of benzylic alcohols, *ACS Catal.* 2 (4) (2012) 622–631.
- [50] X. Xu, et al., Synthesis of palladium nanoparticles supported on mesoporous N-doped carbon and their catalytic ability for biofuel upgrade, *J. Am. Chem. Soc.* 134 (41) (2012) 16987–16990.
- [51] N.M. Julkapli, S. Bagheri, Graphene supported heterogeneous catalysts: an overview, *Int. J. Hydrogen Energy* 40 (2) (2015) 948–979.
- [52] X.-H. Li, M. Antonietti, Metal nanoparticles at mesoporous N-doped carbons and carbon nitrides: functional Mott–Schottky heterojunctions for catalysis, *Chem. Soc. Rev.* 42 (16) (2013) 6593–6604.
- [53] A.S. Nagpure, et al., Hydrogenation of cinnamaldehyde to hydrocinnamaldehyde over Pd nanoparticles deposited on nitrogen-doped mesoporous carbon, *RSC Adv.* 6 (50) (2016) 44333–44340.
- [54] S. Armenise, et al., Elucidation of catalyst support effect for NH₃ decomposition using Ru nanoparticles on nitrogen-functionalized carbon nanofiber monoliths, *J. Phys. Chem. C* 116 (50) (2012) 26385–26395.
- [55] J. Long, K. Shen, Y. Li, Bifunctional N-doped Co@C catalysts for base-free transfer hydrogenations of nitriles: controllable selectivity to primary amines vs imines, *ACS Catal.* 7 (1) (2017) 275–284.
- [56] D.A. Bulushev, et al., Copper on carbon materials: stabilization by nitrogen doping, *J. Mater. Chem. A* 5 (21) (2017) 10574–10583.
- [57] N.K. Raman, M.T. Anderson, C.J. Brinker, Template-based approaches to the preparation of amorphous, nanoporous silicas, *Chem. Mater.* 8 (8) (1996) 1682–1701.
- [58] T.-Z. Ren, et al., Nitric acid oxidation of ordered mesoporous carbons for use in electrochemical supercapacitors, *J. Solid State Electrochem.* 17 (8) (2013) 2223–2233.
- [59] Y. Roman-Leshkov, et al., Production of dimethylfuran for liquid fuels from biomass-derived carbohydrates, *Nature* 447 (2007) 982–985.
- [60] Z. Wu, P.A. Webley, D. Zhao, Comprehensive study of pore evolution, mesostructural stability, and simultaneous surface functionalization of ordered mesoporous carbon (FDU-15) by wet oxidation as a promising adsorbent, *Langmuir* 26 (12) (2010) 10277–10286.
- [61] M.P. Kumar, et al., On the large capacitance of nitrogen doped graphene derived by a facile route, *RSC Adv.* 4 (73) (2014) 38689–38697.
- [62] R. Ryoo, S.H. Joo, S. Jun, Synthesis of highly ordered carbon molecular sieves via template-mediated structural transformation, *J. Phys. Chem. B* 103 (37) (1999) 7743–7746.
- [63] T.V. Kotbagi, et al., Highly efficient nitrogen-doped hierarchically porous carbon supported Ni nanoparticles for the selective hydrogenation of furfural to furfuryl alcohol, *RSC Adv.* 6 (72) (2016) 67662–67668.
- [64] M. Thommes, et al., Physisorption of gases, with special reference to the evaluation of surface area and pore size distribution (IUPAC Technical Report), *Pure Appl. Chem.* 87 (2015).
- [65] J.J.F. Scholten, A.P. Pijpers, A.M.L. Hustings, Surface characterization of supported and unsupported hydrogenation catalysts, *Catal. Rev.* 27 (1) (1985) 151–206.
- [66] Shen, C., et al., The Co-N-C Catalyst Synthesized with a Hard-Template and Etching Method to Achieve Well-Dispersed Active Sites for Ethylbenzene Oxidation. (2296-2646 (Print)).
- [67] Hu, H., et al., Atomically Dispersed Selenium Sites on Nitrogen-Doped Carbon for Efficient Electrocatalytic Oxygen Reduction. (1521-3773 (Electronic)).
- [68] L. Warczinski, et al., Anchoring of palladium nanoparticles on N-doped mesoporous carbon, *Phys. Chem. Phys.* 22 (37) (2020) 21317–21325.
- [69] Z. Shi, et al., Metal-nitrogen-doped carbon materials as highly efficient catalysts: progress and rational design, *Adv. Sci.* 7 (15) (2020) 2001069.
- [70] Y. Marco, et al., Support-induced oxidation state of catalytic Ru nanoparticles on carbon nanofibers that were doped with heteroatoms (O, N) for the decomposition of NH₃, *ChemCatChem* 5 (12) (2013) 3829–3834.
- [71] L. Yue, et al., Efficient CO₂ adsorption on nitrogen-doped porous carbons derived from d-glucose, *Energy Fuels* 32 (6) (2018) 6955–6963.
- [72] H. Mansour, E. Iglesia, Mechanistic connections between CO₂ and CO hydrogenation on dispersed ruthenium nanoparticles, *J. Am. Chem. Soc.* 143 (30) (2021) 11582–11594.
- [73] J. Cored, et al., Hydrothermal synthesis of ruthenium nanoparticles with a metallic core and a ruthenium carbide shell for low-temperature activation of CO₂ to methane, *J. Am. Chem. Soc.* 141 (49) (2019) 19304–19311.
- [74] S. Wang, et al., The role of ruthenium in CO₂ capture and catalytic conversion to fuel by dual function materials (DFM), *Catalysts* 7 (3) (2017).
- [75] Q. Wu, et al., N-doped porous carbon from different nitrogen sources for high-performance supercapacitors and CO₂ adsorption, *J. Alloys Compd.* 786 (2019) 826–838.
- [76] Q. Yu, et al., One-Pot synthesis of N-rich porous carbon for efficient CO₂ adsorption performance, *Molecules* 27 (2022), <https://doi.org/10.3390/molecules27206816>.
- [77] Y. Cao, et al., Metal/porous carbon composites for heterogeneous catalysis: old catalysts with improved performance promoted by N-doping, *ACS Catal.* 7 (12) (2017) 8090–8112.
- [78] A.S. Nagpure, et al., Novel Ru nanoparticle catalysts for the catalytic transfer hydrogenation of biomass-derived furanic compounds, *Sustain. Energy Fuels* 4 (7) (2020) 3654–3667.
- [79] J. vanderWaal, et al., Zeolite titanium beta: a selective catalyst in the meerwein-ponndorf-verley-oppenauer reactions, *Stud. Surf. Sci. Catal.* (1997) 1015–1024.
- [80] Y. Fan, et al., Efficient single-atom Ni for catalytic transfer hydrogenation of furfural to furfuryl alcohol, *J. Mater. Chem. A* 9 (2) (2021) 1110–1118.
- [81] S. Zhou, et al., Zirconium–lignosulfonate polyphenolic polymer for highly efficient hydrogen transfer of biomass-derived oxygenates under mild conditions, *Appl. Catal. B Environ.* 248 (2019) 31–43.
- [82] Y. Xin, et al., Selective 5-hydroxymethylfurfural hydrogenolysis to 2,5-dimethylfuran over bimetallic Pt-FeOx/AC catalysts, *Catalysts* 11 (2021), <https://doi.org/10.3390/catal11080915>.
- [83] R. Goyal, et al., Studies of synergy between metal-support interfaces and selective hydrogenation of HMF to DMF in water, *J. Catal.* 340 (2016) 248–260.